Seismic Performance of Irregular Buildings Through the CASS Method

Andrea Montanino[1(✉)] and Francesco Fabbrocino[2]

[1] International Center for Numerical Methods in Engineering, Carrer del Gran Capità, 08034 Barcelona, Spain
amontanino@cimne.upc.edu

[2] Pegaso Telematic University, Centro Direzionale ISOLA F2, 80143 Naples, Italy
francesco.fabbrocino@unipegaso.it

Abstract. The behavior of masonry structures plays a crucial role in the preservation and conservation of heritage sites, especially in seismically active areas. In this work, the Continuous Airy-based for Stress Singularities (CASS) method is applied to model the response of a masonry façade under different external loading and displacement conditions, including lateral seismic forces.

The formulation of a Boundary Value Problem (BVP) for structures composed of unilateral materials, is briefly recalled, then, the CASS numerical formulation is presented, highlighting its distinctive features, such as its ability to model complex stress distributions, especially dealing with stress concentration over curves. The resulting discrete problem is cast as an optimisation problem with conic discontinuity constraints, which is particularly useful for handling complex geometries, such as those encountered in heritage architecture.

The presented numerical results not only address the calculation of seismic load multipliers—key parameters for evaluating the seismic performance of structures—but help in discussing various numerical aspects, such as convergence issues and the treatment of irregular geometries.

Keywords: Masonry structures · Unilateral materials · Boundary Value Problem · Force-based method

1 Introduction

The preservation and assessment of historic masonry structures, which constitute a significant portion of the world's architectural heritage, have gained increasing attention within the scientific community. Accurate modeling of the mechanical behavior of these structures is essential not only for protecting human lives but also for maintaining the artistic and cultural value they bring, particularly in terms of tourism and historical significance. Given that most of these structures are made from masonry, it is crucial to develop methods that account for the peculiar behavior of this material.

© The Author(s), under exclusive license to Springer Nature Switzerland AG 2026
O. Gervasi et al. (Eds.): ICCSA 2025 Workshops, LNCS 15886, pp. 338–353, 2026.
https://doi.org/10.1007/978-3-031-97576-9_23

The characteristic of masonry material is its ability of withstanding only compressive forces [19,22,23]. Traditional finite element (FE) methods are often inadequate for modeling this behavior [7,46], which necessitates the development of more advanced approaches [2,40,42–45,47].

The seminal work of Heyman, which framed the mechanics of masonry within modern plasticity theory, led to the development of models such as the Normal, Rigid, No-Tension (NRNT) model, where masonry is treated as a no-tension continuum that can resist compression but not tension. In contrast to previously recalled models, requiring accurate material models and parameter identification [12], Heyman's model does not require the identification of any material parameter [5,20].

A significant challenge in modeling masonry is dealing with stress singularities—lines, or surfaces, where stress concentrates. In the framework of the Heyman material, several strategies have been proposed to capture stress singularities, in the framework of domes and vaults [11,33,38,39], and in the framework of planar masonry buildings, both following displacement-based approaches [16,21,24–27], and force-based approaches [3,6,9,10,29,36,37].

Restricting to masonry façdes, the Continuous Airy-based method for Stress Singularities (CASS) has been recently introduced for the mesh-independent identification of stress patterns [30].

A key point of the CASS method is the computation of curvature within Finite Elements, which is not a common theme in the literature. Several possibilities have been presented in the literature, among which the adoption of averaged value across more elements [17,35], or adopting higher-order plate-type elements, as in the case of Isogeometric Analysis (IGA) [15], to improve continuity and reduce computational complexity. The last technique, in particular, introduces an unnecessary continuity for the Airy stress potential which potentially limits the space of possible solutions of the Boundary Value Problem.

A particularly useful characteristic of the CASS approach is its ability to determine in a fast manner the load-bearing capacity of masonry structures [28,34], by identifying the maximum load multiplier for which an equilibrated solution exists. From this point, it is possible to determine the in-plane mechanisms of the structures [1,8,13,14,41].

Building on these insights, this paper recalls the quadrilateral plate-type FE formulation proposed in [31], designed to model complex, curved in-plane masonry structures, such as arches and buttresses. This formulation provides an optimal balance between accuracy and computational efficiency, addressing the limitations of traditional FE methods and enabling the analysis of a broader range of masonry geometries.

The paper is organized as follows: Sect. 2 provides the theoretical background of the proposed formulation; Sect. 3 recalls briefly the numerical formulation for the case of generically-shaped quadrilateral plate-type FE, detailing the computation of curvature components; Sect. 4 validates the method on an irregular masonry façade under permanent and accidental loads, estimating the seismic

performance, and discussing several numerical issues. Finally, in Sect. 5, conclusions and future developments are discussed.

2 Boundary Value Problem

In this Section, the Boundary Value Problem for masonry structure is briefly recalled, together with the main ingredients needed to develop the CASS methodology.

A domain $\Omega \in \mathrm{R}^2$, as presented in Fig. 1, is considered, with boundary $\partial\Omega$ partitioned in a loaded part $\partial\Omega_N$ and a constrained part $\partial\Omega_D$, such that $\partial\Omega_N \cap \partial\Omega_D = \emptyset$ and $\partial\Omega_N \cup \partial\Omega_D = \partial\Omega$.

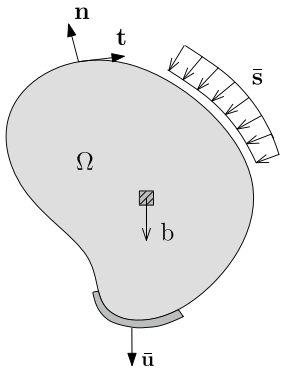

Fig. 1. Domain of the Boundary Value Problem with main notation.

The boundary value problem on Ω is represented by the equilibrium conditions, the kinematic conditions and a constitutive law. The equilibrium equations are

$$\nabla \cdot \mathbf{T} + \mathbf{b} = \mathbf{0} \quad , \qquad \mathbf{x} \in \Omega \tag{1a}$$

$$\mathbf{T}\mathbf{n} = \bar{\mathbf{s}} \qquad \mathbf{x} \in \partial\Omega_N \tag{1b}$$

where $\mathbf{T}$ is the stress tensor, $\mathbf{b}$ is the volume load, $\mathbf{n}$ is the boundary outward normal, and $\bar{\mathbf{s}}$ is the assigned boundary load on $\partial\Omega_N$.

The kinematic conditions are

$$\mathbf{E} = \frac{1}{2}\left(\nabla\mathbf{u} + \nabla\mathbf{u}^T\right) \quad , \qquad \mathbf{x} \in \Omega \tag{2a}$$

$$\mathbf{u} = \bar{\mathbf{u}} \qquad \mathbf{x} \in \partial\Omega_D \tag{2b}$$

being $\mathbf{E}$ the strain tensor, $\mathbf{u}$ the displacement field, and $\bar{\mathbf{u}}$ the prescribed displacement at the constrained boundary $\partial\Omega_D$.

The constitutive relation for the masonry material is represented by the Heyman assumption of a Normal, Rigid, No-Tension (NRNT) material, expressed as

$$\mathbf{T} \in \mathrm{Sym}^{-} \quad , \tag{3a}$$

$$\mathbf{E} \in \mathrm{Sym}^{+} \quad , \tag{3b}$$

$$\mathbf{T} \cdot \mathbf{E} = 0 \quad , \tag{3c}$$

where (3a) expresses the no tension material requirement, (3b) the indeformability in compression, and (3c) the normality condition, that is, the infinite friction condition.

This boundary value problem can be recast into an optimisation problem by introducing the Total Potential Energy

$$\mathcal{E}_p(\mathbf{u}) = \frac{1}{2}\int_{\Omega} \mathbf{T} \cdot \mathbf{E} d\Omega - \int_{\partial\Omega_N} \bar{\mathbf{s}} \cdot \mathbf{u} dA - \int_{\Omega} \mathbf{b} \cdot \mathbf{u} d\Omega \tag{4}$$

or the Total Complementary Energy

$$\mathcal{E}_c(\mathbf{T}) = \frac{1}{2}\int_{\Omega} \mathbf{T} \cdot \mathbf{E} d\Omega - \int_{\partial\Omega_D} \mathbf{T}\mathbf{n} \cdot \bar{\mathbf{u}} d\Omega \tag{5}$$

From these energies, two different solution strategies can be developed [32]: the minimisation of the Total Potential Energy with respect to the unknown field $\mathbf{u}$ gives rise to a displacement-based approach; the minimisation of the Total Complementary Energy with respect to the stress field $\mathbf{T}$ originates a force- or stress-based approach.

In this work, the latter strategy is considered: the minimisation problem, therefore, is written as

$$\mathcal{E}_c(\mathbf{T}^*) = \min_{\mathbf{T} \in \mathcal{H}} \mathcal{E}_c(\mathbf{T}) \quad , \tag{6}$$

with

$$\mathcal{H} = \left\{ \mathbf{T} \in \mathrm{SBV} \text{ s.t. } \mathbf{T} \in \mathrm{Sym}^{-} , \nabla \cdot \mathbf{T} + \mathbf{b} = \mathbf{0} , \mathbf{T}\mathbf{n} = \bar{\mathbf{s}} \right\} \tag{7}$$

the set of admissible stress fields, that is, compliant with the internal and external equilibrium (1), and with the material restriction (3a).

Furthermore, given the normality condition (3c), the objective function

$$\mathcal{E}_c(\mathbf{T}) = -\int_{\partial\Omega_D} \mathbf{T}\mathbf{n} \cdot \bar{\mathbf{u}} d\Omega \tag{8}$$

is a linear functional.

The formulation (6)-(7), in its present form involving directly the stress field, in any discretized version, would bring to a problem with a high number of equality constraints, corresponding to all the evaluations of the equilibrium condition. Therefore, it is useful to rewrite it adopting the Airy stress potential F, that is, a

scalar function intrinsically complying with the equilibrium condition. The Airy stress potential is formulated as a scalar function

$$\mathrm{F} \in C^0 \quad \text{s.t.} \quad \mathbf{T} = \mathbf{R}^T \mathbf{H}(\mathrm{F}) \mathbf{R} + \mathbf{B}_\mathrm{F} \,, \tag{9}$$

with $\mathbf{H}$ the Hessian operator, $\mathbf{R}$ is a skew-symmetric operator representing a counterclockwise rotation of $\pi/2$, and $\mathbf{B}_\mathrm{F}$ a tensor accounting for the specific internal load distribution $\mathbf{b}$, such that

$$\nabla \cdot \mathbf{B}_\mathrm{F} = -\mathbf{b} \,. \tag{10}$$

Equations (9) and (10), particularised to the Cartesian reference frame, read in the form

$$\mathrm{T}_{xx} = \mathrm{F}_{,yy} \,, \quad \mathrm{T}_{yy} = \mathrm{F}_{,xx} \,, \mathrm{T}_{xy} = -\mathrm{F}_{,xy} + b_y x + b_x y \,, \tag{11}$$

being T_{xx}, T_{yy}, and T_{xy} the Cartesian components of the stress tensor $\mathbf{T}$, and b_x and b_y the Cartesian components of the internal volume load $\mathbf{b}$. Moreover, a Latin letter following a comma, as a subscript, represents partial derivative. Replacing (11) into the internal equilibrium condition (1a) allows for checking the correct definition of the Airy stress potential.

Therefore, Problem (6)-(7) is reformulated in terms of the Airy stress potential as

$$\mathcal{E}_c(\mathrm{F}^*) = \min_{\mathrm{F} \in \mathcal{H}_\mathrm{F}} \mathcal{E}_c(\mathrm{F}) \quad , \tag{12}$$

being $\mathcal{H}_\mathrm{F}$ the set of admissible Airy stress potentials, univocally determined from $\mathcal{H}$.

The material constraints transform into a condition on the Hessian of the Airy stress potential, specifically

$$\mathbf{R}^T \mathbf{H}(\mathrm{F}) \mathbf{R} + \mathbf{B}_\mathrm{F} \in Sym^- \tag{13}$$

that is, in a Cartesian reference frame,

$$\mathrm{F}_{,xx} + \mathrm{F}_{,yy} \leq 0 \,, \quad \mathrm{F}_{,xx}\, \mathrm{F}_{,yy} - \left(-\mathrm{F}_{,xy} + \mathrm{b}_\mathrm{F}\right)^2 \geq 0 \,. \tag{14}$$

It is worth noting that, in the absence of volume forces, condition (13) has an immediate geometrical meaning, since the Hessian of a function is strictly linked to its curvature. Therefore, the Airy stress potential for a domain composed of a unilateral material must have a negative, semi-definite Hessian in each point, and therefore, be point-wise concave.

Concerning boundary conditions, the Airy-based formulation transforms the boundary equilibrium into

$$\mathbf{R}^T \mathbf{H}(\mathrm{F}) \mathbf{R} \mathbf{n} + \mathbf{B}_\mathrm{F} \mathbf{n} = \bar{\mathbf{s}} \quad , \tag{15}$$

and, denoting with

$$\mathrm{T}_{nn} = \mathbf{n} \cdot \mathbf{T} \mathbf{n} \,, \quad \mathrm{T}_{nt} = \mathbf{t} \cdot \mathbf{T} \mathbf{n} \quad , \tag{16}$$

the normal and tangential components of the emerging stress at the boundary, with $\mathbf{t}$ and $\mathbf{n} = \mathbf{R}\mathbf{t}$ the unit vectors tangent and orthogonal to the boundary itself, the boundary conditions can be finally rewritten as

$$\mathrm{T}_{nn} = \bar{\mathbf{s}} \cdot \mathbf{n} = \mathbf{t} \cdot \mathbf{H}(\mathrm{F})\mathbf{t} + \mathbf{n} \cdot \mathbf{B}_{\mathrm{F}}\mathbf{n} = \mathrm{F}_{,tt} - 2\mathrm{b}_{\mathrm{F}} t_x t_y \quad (17a)$$

$$\mathrm{T}_{nt} = \bar{\mathbf{s}} \cdot \mathbf{t} = -\mathbf{n} \cdot \mathbf{H}(\mathrm{F})\mathbf{t} + \mathbf{t} \cdot \mathbf{B}_{\mathrm{F}}\mathbf{n} = -\mathrm{F}_{,nt} + \mathrm{b}_{\mathrm{F}}(t_x^2 - t_y^2) \quad (17b)$$

being t_x, t_y the Cartesian components of $\mathbf{t}$.

3 The Continuous Airy-Based for Stress Singularities

In this Section the main points of the numerical formulation proposed in [31] are recalled, starting from the domain discretisation until the discrete formulation of the optimisation problem (12).

The domain is decomposed in quadrilateral plate-type finite elements, with four nodes in correspondence of its corner, as depicted in Fig. 2b; each node is provided with three degrees of freedom, specifically the unknown function value ϕ and its first derivatives in the Cartesian directions $\phi_{,x}$ and $\phi_{,y}$. This assures the discretisation being C^1-continuous at the nodes, and only C^0-continuous across the element boundary, since this discretisation cannot assure continuity of the normal derivative at the elements' interfaces.

For generalisation purposes, each element is mapped into a square element, referred to as as parent element, in a parent reference frame $\{0, s, t\}$, such that $0 < s < 1$, and $0 < t < 1$, as shown in Fig. 2.

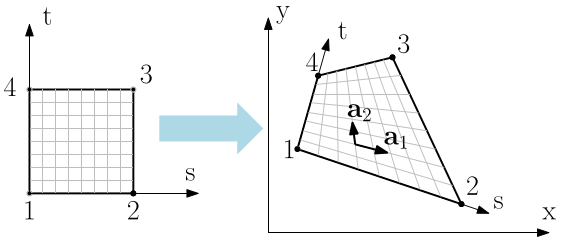

Fig. 2. Mapping between the parent and real geometries.

Since each element is provided with a total of 12 degrees of freedom, the interpolant function $\phi(x(s,t), y(s,t))$ is generated through the scalar product of a coefficient vector $\hat{\mathbf{w}} = [w_1, ...w_{12}]^T$ and a monomial basis

$$\mathbf{p}^T(s,t) = \left[1, s, t, s^2, st, t^2, s^3, s^2t, st^2, t^3, s^3t, st^3\right] , \quad (18)$$

such that

$$\phi(x(s,t), y(s,t)) = \mathbf{p}^T(s,t)\hat{\mathbf{w}} \quad , \quad (19)$$

The coefficient vector $\hat{\mathbf{w}}$ can be rewritten in terms of the nodal degrees of freedom

$$\hat{\boldsymbol{\phi}} = [\hat{\phi}^1, \hat{\phi}^1{}_{,x}\,, \hat{\phi}^1{}_{,y}\,, ..., \hat{\phi}^4, \hat{\phi}^4{}_{,x}\,, \hat{\phi}^4{}_{,y}\,] \tag{20}$$

after a suitable interpolation of $\phi(x(s,t), y(s,t))$, on the original element shape, with the nodal degrees of freedom, represented by 12 conditions in the form

$$\phi\Big|^i = \hat{\phi}^i\,, \quad \phi_{,x}\,\Big|^i = \hat{\phi}^i{}_{,x}\,, \quad \phi_{,y}\,\Big|^i = \hat{\phi}^i{}_{,y}\,, \tag{21}$$

with $i = 1, .., 4$, and collected in compact form as

$$\hat{\boldsymbol{\phi}} = \mathbf{B}\hat{\mathbf{w}} \quad . \tag{22}$$

By inverting (22) and combining with (19), the final interpolation function is

$$\phi(x(s,t), y(s,t)) = \mathbf{p}^T(s,t)\mathbf{B}^{-1}(\hat{\mathbf{x}})\hat{\boldsymbol{\phi}}\,. \tag{23}$$

By recalling from Sect. 2 that the curvature of the unknown function is required to compute the stress, first of all, it has to be noticed that the curvature is not continuous at the element nodes, therefore, it must be computed on internal points, referred to as control points. In this work, the points with local coordinates

$$\begin{aligned} \bar{s}_1 &= 0.25\,, \quad \bar{t}_1 = 0.25 \\ \bar{s}_2 &= 0.75\,, \quad \bar{t}_2 = 0.25 \\ \bar{s}_3 &= 0.75\,, \quad \bar{t}_3 = 0.75 \\ \bar{s}_4 &= 0.25\,, \quad \bar{t}_4 = 0.75 \end{aligned} \tag{24}$$

are selected, represented in Fig. 3.

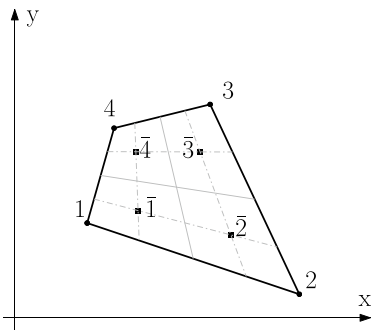

Fig. 3. Position of the control points on a generic element. The control points are placed at the centres of each quadrant in which the element is partitioned.

The Hessian tensor $\mathbf{H}(\phi)$ is expressed, following the curvilinear reference frame adopted of Fig. 2b, as

$$\mathbf{H} = (\nabla\phi)_{,\alpha} \otimes \mathbf{a}^\alpha\,, \tag{25}$$

with $\mathbf{a}^\alpha$, $\alpha = 1, 2$ the contravariant basis of the curvilinear reference system. Then the Hessian is projected onto the Cartesian directions as

$$\mathrm{H}_{ij} = [(\nabla\phi)_{,\alpha} \cdot \mathbf{e}_i](\mathbf{a}^\alpha \cdot \mathbf{e}_j)\,. \tag{26}$$

In Eqs. 25-(26) the derivation with respect to α means partial derivative with respect to the curvilinear directions s, t, respectively.

After some algebra (with details reported in [31]), the final expressions of the Cartesian components of the curvature can be expressed in terms of the nodal unknowns as

$$\begin{aligned} \phi_{,xx} &= \mathbf{h}_{xx}^T \mathbf{B}^{-1} \hat{\boldsymbol{\phi}} \\ \phi_{,yy} &= \mathbf{h}_{yy}^T \mathbf{B}^{-1} \hat{\boldsymbol{\phi}} \\ \phi_{,xy} &= \mathbf{h}_{xy}^T \mathbf{B}^{-1} \hat{\boldsymbol{\phi}} \end{aligned} \tag{27}$$

being $\mathbf{h}_{xx}$, $\mathbf{h}_{yy}$, and $\mathbf{h}_{xy}$ vector functions depending on the curvilinear coordinates and on the element mapping.

3.1 BVP Discretisation

Given the procedure recalled in the previous Section, here some discussion on the discretisation of the BVP is addressed.

In particular, the Total Complementary Energy (8) in terms of the Airy stress potential is given by

$$\mathcal{E}_c(\mathrm{F}) = -\int_{\partial\Omega_D} \left(\mathbf{R}^T \mathbf{H}(\mathrm{F}) \mathbf{R} + \mathbf{B}_\mathrm{F}\right) \mathbf{n} \cdot \bar{\mathbf{u}} ds\,, \tag{28}$$

which is written in terms of the second derivatives of the Airy stress potential, which are not degrees of freedom in the present formulation. However, by integrating Eq. (28) along the DIrichlet boundary, it comes out, after discretisation, that

$$\begin{aligned} \mathcal{E}_c(\hat{\mathbf{F}}) =& [F_{,t}\,\big|_1 - F_{,t}\,\big|_2 - 2\mathrm{b_F} t_x t_y \Delta s]\bar{u}_n \\ &+ [F_{,n}\,\big|_2 - F_{,n}\,\big|_1 - \mathrm{b_F}(t_x^2 - t_y^2)\Delta s]\bar{u}_t\,, \end{aligned} \tag{29}$$

with $\bar{u}_t$ and $\bar{u}_n$ the normal and tangent boundary settlement in tangential $\mathbf{t}$ and normal $\mathbf{n}$ direction, respectively. Equation (29), summed up on all the elements of the Dirichlet boundary, represents the discretised objective function. $F_{,t}$ and $F_{,n}$ can be further rewritten in terms of the Cartesian components of the gradient of the Airy stress potential at the nodes of the discretisation.

The negative semi-definiteness of the stress in the domain is just checked by evaluating the stress in the elements' control points, that is, evaluating (14) through (27). Therefore, the material constraints transform into a set of coninc constraints in the form

$$\begin{aligned} (\mathbf{h}_{xx}^T + \mathbf{h}_{yy}^T)\mathbf{B}^{-1}\hat{\mathbf{F}} &\leq 0 \\ (\mathbf{h}_{xx}^T \mathbf{B}^{-1}\hat{\mathbf{F}})(\mathbf{h}_{yy}^T \mathbf{B}^{-1}\hat{\mathbf{F}}) - ((\mathbf{h}_{yy}^T \mathbf{B}^{-1}\hat{\mathbf{F}}) - b(\mathbf{x}))^2 &\geq 0 \end{aligned} \tag{30}$$

Relations (30), collected for all the control points, form a set of coninc disequality constraints, that can be written in the form

$$f(\hat{\mathbf{F}}) \geq \mathbf{0} \tag{31}$$

The last ingredient is the imposition of the boundary conditions (17). Again, here second derivative of the unknown function appears, which are not among the degrees of freedom, therefore, the most convenient step is the integration of emerging stresses across the element boundary, realizing not a point-wise equilibrium on the element side, but an equilibrium of the stress resultant, that can be understood also as an average equilibrium at the elementary level. This formulation, however, converges to the point-wise equilibrium with the reduction of the mesh size.

Therefore, Eqs. (17) are rewritten as

$$\mathbf{R}_n = \int_{\partial\Omega_{el}} \mathrm{F}_{,tt} - 2\mathrm{b_F} t_x t_y \tag{32a}$$

$$\mathbf{R}_t = -\int_{\partial\Omega_{el}} \mathrm{F}_{,nt} + \mathrm{b_F}(t_x^2 - t_y^2) \tag{32b}$$

with $\mathbf{R}_n$ and $\mathbf{R}_t$ the resultant of the applied load along the element boundary in the normal and tangential directions, respectively.

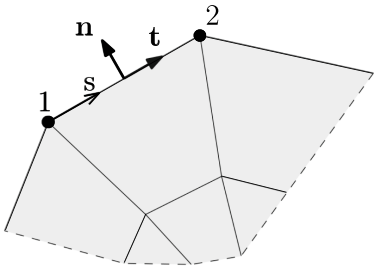

Fig. 4. Geometry of a boundary element and main notation.

After some algebra, and introducing the nodal degrees of freedom, the final boundary conditions at the element boundary are

$$\begin{aligned} F_{,t}\big|_2 - F_{,t}\big|_1 \quad &= T_{nn}\Delta s + \\ &- b_y t_x t_y (x_1 + x_2)\Delta s + \\ &- b_x t_x t_y (y_1 + y_2)\Delta s \end{aligned} \tag{33}$$

$$\begin{aligned} F_{,n}\big|_2 - F_{,n}\big|_1 \quad &= -T_{nt}\Delta s \\ &+ \frac{1}{2} b_y (t_x^2 - t_y^2)(x_1 + x_2)\Delta s \\ &+ \frac{1}{2} b_x (t_x^2 - t_y^2)(y_1 + y_2)\Delta s \end{aligned} \tag{34}$$

where Δs is the element's boundary length, and x_1, x_2, y_1, y_1 are the coordinates of the two extreme points of the element's boundary, as represented in Fig. 4.

Equations (33)-(34) can be written as linear expression of the degrees of freedom, as

$$\mathbf{K}_{\partial\Omega}\hat{\mathbf{F}} = \hat{\mathbf{s}} \tag{35}$$

and finally, by collecting Eqs. (29), (31), and (35), for all the evaluations required, the final, discrete form of the optimisation problem is

$$\begin{aligned} E_c(\hat{\mathbf{F}}^0) \quad &= \min E_c(\hat{\mathbf{F}}) \\ \text{s.t.} \quad & f(\hat{\mathbf{F}}) \leq \mathbf{0} \\ & \mathbf{K}_{\partial\Omega}\hat{\mathbf{F}} = \hat{\mathbf{s}} \end{aligned} \tag{36}$$

Following the same discretisation strategy, but slightly changing the problem formulation, it is possible to compute the maximum - or minimum - admissible load on a masonry structure by parametrizing the external load through a coefficient λ, such that

$$\hat{\mathbf{s}} = \hat{\mathbf{s}}_0 + \lambda\hat{\mathbf{s}}_v \tag{37}$$

with $\hat{\mathbf{s}}_0$ the permanent loads, and $\hat{\mathbf{s}}_v$ the variable part of the load, related, for example, to a seismic action, or to accidental loads.

In this case, the optimisation problem is reformulated as

$$\begin{aligned} \lambda^0 \quad &= \min \lambda \\ \text{s.t.} \quad & f(\hat{\mathbf{F}}) \leq \mathbf{0} \\ & \mathbf{K}_{\partial\Omega}\hat{\mathbf{F}} = \hat{\mathbf{s}}_0 + \lambda\hat{\mathbf{s}}_v \end{aligned} \tag{38}$$

4 Numerical Examples

In this Section a non-symmetric structure is considered, under the action of permanent loads, in which the formation of possible load patterns are observed, and under the effect of horizontal loads, to determine the maximum load multiplier and the corresponding seismic performance of the structure.

The geometry of the masonry façade is represented in Fig. 5, with its geometrical dimensions.

The permanent loads on the top side is $q = 25$ kN/m, while the self-weight is of 18 kN/m^2. Additionally, two variable loads on the vertical sides of the structures are considered, representative of seismic actions.

Effect of Permanent Loads. The analysis under the effect of the load on the top side of the structure, and of the self-weight, reveals the stress patterns,in terms of minimum principal stress, depicted in Fig. 6.

In particular, it may be observed the formation of singularities above the lintel of the window on the right side, as well of a singularity until the lower corners of the façade.

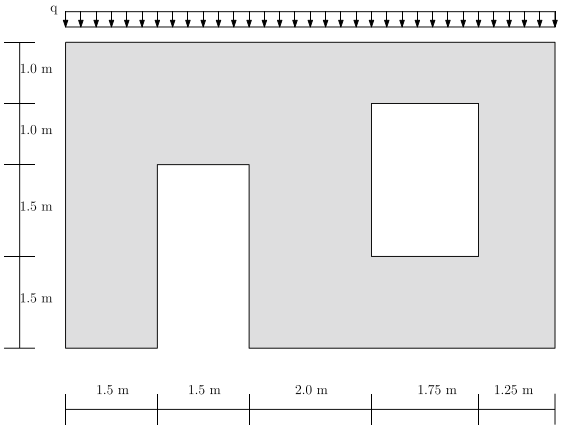

Fig. 5. Unsymmetric façade - geometry and dimensions.

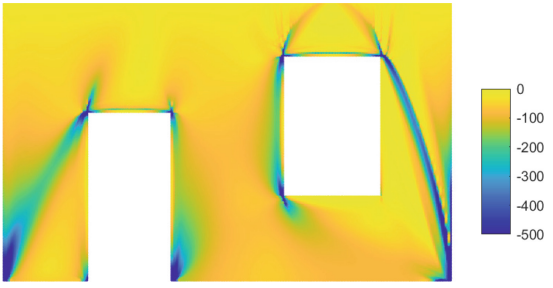

Fig. 6. Unsymmetric façade - stress pattern for the only permanent loads.

The equilibrium of this geometry under the vertical loads is got introducing a precompressive loads on the left and right sides of the structure, in the form of a normal, homogeneous load $q_s = 5.07$ kN/m, corresponding to an horizontal force $F_H = 25$ kN, which is however not relevant, from a practical point of view, with respect to the total vertical load, represented by the combination of the self-weight and the upper load, which sums to $F_V = 750$ kN, being therefore the ratio $F_H/F_V = 0.033$

Seismic Loads. For checking the seismic performance of the structure, an equivalent horizontal load has been simulated at the left and right sides of the structures, and increased until an equilibrated solution is found.

By solving (38) for the case of the seismic load on the left side of the structure, and considering a permanent load $q_{s,l} = 150$ kN/m (that is, the total vertical load acting on the façade), a maximum value for the seismic multiplier is $\lambda = 0.55$, which also stands for the so called Peak Ground Acceleration (PGA), a seismic indicator measuring the maximum soil acceleration that a structure can withstand. The corresponding stress pattern is depicted in Fig. 7, where stress

singularities are visible, in the form of preferential stress paths going to the lower, right corners of the structure (against the left side of the door, and of the right part of the façade). This stress pattern also suggests possible rocking mechanisms of the structure. The presence of unloaded zones, or of zones under monoaxial stress patterns, also suggest the possible formation of cracks without loss of energy for the structure.

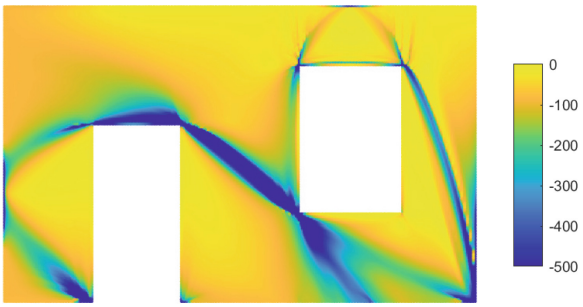

Fig. 7. Unsymmetric façade - stress pattern for the permanent and equivalent seismic load from the left side.

Repeating the simulation for the same variable load, but on the right side, the maximum value of the seismic multiplier is $\lambda = 0.586$, whose corresponding stress pattern is reported in Fig. 8. Also in this case, stress singularities pointing against the lower corners of the structure are present, suggesting the formation of other rocking mechanisms which however are coherent with the imposed load and the structure geometry.

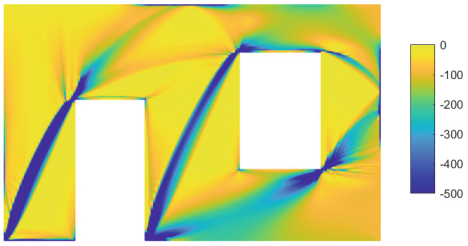

Fig. 8. Unsymmetric façade - stress pattern for the permanent and equivalent seismic load from the right side.

A further comment is proposed concerning the difference between the values of λ in the two cases. This slight difference, already observed in [4], even though for a different type of horizontal load, is due to the unsymmetry of the structure, which naturally leads to different load multipliers.

5 Conclusion

In this paper, the Continuous Airy-based method for Stress Singularities (CASS) is applied to determine the seismic multiplier on unsymmetric façades. After recalling the theorical fundamentals of the Boundary Value Problem, and of the discretisation strategy in the CASS method, with particular focus on the curvature computation on non-rectangular finite elements, the CASS method is applied to a non-symmetric structure to determine possible stress patterns under self-weight, and under the effects of seismic loads.

Specifically, the non-symmetry of the load multiplier, following the unsymmetry of the structure, is evidenced, as well as the need for a suitable numerical prestress at the sides of the structure to simulate the effects of the vertical loads.

Future developments of this work will involve out-of-plane mechanisms, which are well developed with displacement-based approaches [18], but still need to be approached from a force-based perspective.

Disclosure of Interests. There is no competing interest to declare.

References

1. Buzzetti, M., Gandolfi, A., Pingaro, N., Milani, G.: A new advanced and simple procedure for the nonlinear static analysis of curved masonry structures. In: International Conference on Protection of Historical Constructions, pp. 176–183. Springer (2025)
2. Alfano, G., Rosati, L., Valoroso, N.: A numerical strategy for finite element analysis of no-tension materials. Int. J. Numer. Methods Eng. **48**(3), 317–350 (2000). https://doi.org/10.1002/(SICI)1097-0207(20000530)48:3<317::AID-NME868>3.0.CO;2-C
3. Angelillo, M.: Constitutive relations for no-tension materials. Meccanica **28**, 195–202 (1993). https://doi.org/10.1007/BF00989121
4. Angelillo, M., Iannuzzo, A., Montanino, A.: Discretised continuum approaches: from continuum to dis-continuum. In: Discrete Computational Mechanics of Masonry Structures, pp. 95–163. Springer (2023). https://doi.org/10.1007/978-3-031-32476-5_3
5. Angelillo, M. (ed.): Mechanics of Masonry Structures. CICMS, vol. 551. Springer, Vienna (2014). https://doi.org/10.1007/978-3-7091-1774-3
6. Baratta, A., Corbi, O.: Stress analysis of masonry vaults and static efficacy of FRP repairs. Int. J. Solids Struct. **44**(24), 8028–8056 (2007). https://doi.org/10.1016/j.tafmec.2005.09.008
7. Block, P., Ciblac, T., Ochsendorf, J.: Real-time limit analysis of vaulted masonry buildings. Comput. Struct. **84**(29–30), 1841–1852 (2006). https://doi.org/10.1016/j.compstruc.2006.08.002
8. Buzzetti, M., Pingaro, N., Gandolfi, A., Milani, G.: Limit analysis-based approach for the assessment of local failures in masonry aggregates according to Italian standards. In: International Conference on Protection of Historical Constructions, pp. 168–175. Springer (2025)

9. Crespino, E., Adriaenssens, S., Fraddosio, A., Olivieri, C., Piccioni, M.D.: A multi-objective optimization approach for novel shell/frame systems under seismic load. Structures **65**, 106625 (2024)
10. Cuomo, M., Ventura, G.: A complementary energy formulation of no tension masonry-like solids. Comput. Methods Appl. Mech. Eng. **189**(1), 313–339 (2000). https://doi.org/10.1016/S0045-7825(99)00298-4
11. Cusano, C., Montanino, A., Olivieri, C., Paris, V., Cennamo, C.: Graphical and analytical quantitative comparison in the Domes assessment: the case of San Francesco di Paola. Appl. Sci. **11**(8), 3622 (2021). https://doi.org/10.3390/app11083622
12. Di Gennaro, L., et al.: In-situ load testing of an ancient masonry structure using fibre optics. Structures **70**, 107567 (2024)
13. Di Gennaro, L., Guadagnuolo, M., Monaco, M.: Rocking analysis of towers subjected to horizontal forces. Buildings **13**(3), 762 (2023)
14. Fabbrocino, F., Olivieri, C., Luciano, R., Vaiano, G., Maddaloni, G., Iannuzzo, A.: Seismic performance of historic masonry buildings: a comparative analysis of equivalent frame and block-based methods. Alex. Eng. J. **109**, 359–375 (2024)
15. Farahat, A., Verhelst, H.M., Kiendl, J., Kapl, M.: Isogeometric analysis for multi-patch structured Kirchhoff-Love shells. Comput. Methods Appl. Mech. Eng. **411**, 116060 (2023)
16. Ferrero, C., Cusano, C., Yavuzer, M.N., Wu, Y.X., Iannuzzo, A.: When cracks are (not) a structural concern: the case of 'Giovanni Vinciguerra' School in Anagni. Int. J. Masonry Res. Innov. **7**(1–2), 217–232 (2022)
17. Fraternali, F., Angelillo, M., Fortunato, A.: A lumped stress method for plane elastic problems and the discrete-continuum approximation. Int. J. Solids Struct. **39**(25), 6211–6240 (2002)
18. Frunzio, G., Di Gennaro, L.: The out of plane behaviour of masonry infilled frames. J. Phys. Conf. Ser. **2090**(1), 012148 (2021)
19. Guadagnuolo, M., Di Gennaro, L., Basile, A., De Matteis, G.: Simplified methods for the evaluation of mechanical properties of tuff masonry walls in Campania (Italy). Procedia Struct. Integr. **44**, 878–885 (2023)
20. Heyman, J.: The stone skeleton. Int. J. Solids Struct. **2**(2), 249–279 (1966). https://doi.org/10.1016/0020-7683(66)90018-7
21. Hua, Y., Buzzetti, M., Pingaro, N., da Silva, L.C., Milani, G.: A computerized tool for the kinematic limit analysis of 2D masonry structures failing on a tilting table. SoftwareX **30**, 102180 (2025)
22. Huerta, S.: The analysis of masonry architecture: a historical approach: to the memory of professor Henry. J. Cowan. Archit. Sci. Rev. **51**(4), 297–328 (2008). https://doi.org/10.3763/asre.2008.5136
23. Huerta Fernández, S.: Mechanics of masonry vaults: the equilibrium approach (2001)
24. Iannuzzo, A., et al.: Modelling the cracks produced by settlements in masonry structures. Meccanica **53**(7), 1857–1873 (2017). https://doi.org/10.1007/s11012-017-0721-2
25. Iannuzzo, A., Musone, V., Ruocco, E.: A neural network-based automated methodology to identify the crack causes in masonry structures. Comput. Aided Civ. Infrastruct. Eng. **39**(24), 3769–3785 (2024). https://doi.org/10.1111/mice.13311
26. Iannuzzo, A.: Energy based fracture identification in masonry structures: the case study of the church of "Pietà dei Turchini". J. Mech. Mater. Struct. **14**(5), 683–702 (2019). https://doi.org/10.2140/jomms.2019.14.683

27. Iannuzzo, A., Mallardo, V.: A novel approach to model differential settlements and crack patterns in masonry structures. Eng. Struct. **323**, 119220 (2025). https://doi.org/10.1016/j.engstruct.2024.119220
28. Iannuzzo, A., Montanino, A.: A limit analysis-based CASS approach for the in-plane seismic capacity of masonry façades. Int. J. Solids Struct. **289**, 112633 (2024). https://doi.org/10.1016/j.ijsolstr.2023.112633
29. Lucchesi, M., Šilhavỳ, M., Zani, N.: A new class of equilibrated stress fields for no-tension bodies. J. Mech. Mater. Struct. **1**(3), 503–539 (2006). https://doi.org/10.2140/jomms.2006.1.503
30. Montanino, A., De Gregorio, D., Olivieri, C., Iannuzzo, A.: The continuous airy-based for stress-singularities (CASS) method: an energy-based numerical formulation for unilateral materials. Int. J. Solids Struct. **256**, 111954 (2022). https://doi.org/10.1016/j.ijsolstr.2022.111954
31. Montanino, A., Iannuzzo, A.: A quadrilateral plate-type finite element to model stress singularities in no-tension materials. Comput. Methods Appl. Mech. Eng. **432**, 117433 (2024). https://doi.org/10.1016/j.cma.2024.117433
32. Montanino, A., Olivieri, C., De Gregorio, D., Iannuzzo, A., et al.: Two continuous dual strategies to solve the kinematical and equilibrium problem for masonry-like structures. In: WCCM-ECCOMAS CONGRESS. Scipedia SL (2022)
33. Montanino, A., Olivieri, C., Zuccaro, G., Angelillo, M.: From stress to shape: equilibrium of cloister and cross vaults. Appl. Sci. **11**(9), 3846 (2021). https://doi.org/10.3390/app11093846
34. Montanino, A., Perelli, F.L., De Gregorio, D., Zuccaro, G.: Application of the continuous airy-based for stress singularities (CASS) to the load bearing capacity of masonry structures under seismic loads. In: 9th International Conference on Computational Methods in Structural Dynamics and Earthquake Engineering Methods in Structural Dynamics and Earthquake Engineering (2023). https://doi.org/10.7712/120123.10577.21347
35. Nguyen-Xuan, H., Rabczuk, T., Bordas, S., Debongnie, J.F.: A smoothed finite element method for plate analysis. Comput. Methods Appl. Mech. Eng. **197**(13-16), 1184–1203 (2008). j.cma.2007.10.008
36. Nodargi, N.A.: An isogeometric collocation method for the static limit analysis of masonry domes under their self-weight. Comput. Methods Appl. Mech. Eng. **416**, 116375 (2023). https://doi.org/10.1016/j.cma.2023.116375
37. Olivieri, C.: FORMERLY-Math: constrained form-finding through membrane equilibrium analysis in Mathematica. Softw. Impacts **16**, 100512 (2023). https://doi.org/10.1016/j.simpa.2023.100512
38. Olivieri, C., Cocking, S., Fabbrocino, F., Iannuzzo, A., Placidi, L., Adriaenssens, S.: Seismic capacity of purely compressed shells based on Airy stress function. Continuum Mech. Thermodyn. **37**(2), 21 (2025)
39. Olivieri, C., Fortunato, A., DeJong, M.: A new membrane equilibrium solution for masonry railway bridges: the case study of Marsh Lane Bridge. Int. J. Masonry Res. Innov. **6**(4), 446–471 (2021)
40. Paris, V., Gobbin, F., Nannei, V.M., Resmini, M., Mirabella Roberti, G.: Distinct element method analyses for damage assessment: the Northern Spur of Valverde Bulwark in the Venetian Fortress of Bergamo. Int. J. Archit. Herit., 1–15 (2024)
41. Perelli, F.L., De Gregorio, D., Montanino, A., Olivieri, C., Maddaloni, G., Iannuzzo, A.: Energy-based modelling of in-plane fragility curves for the 2D ultimate capacity of Italian masonry buildings. Front. Built Environ. **9**, 1127523 (2023)

42. Petracca, M., Camata, G., Spacone, E., Pelà, L.: Efficient constitutive model for continuous micro-modeling of masonry structures. Int. J. Archit. Herit. **17**(1), 134–146 (2023). https://doi.org/10.1080/15583058.2022.2124133
43. Prosperi, A., Longo, M., Korswagen, P.A., Korff, M., Rots, J.G.: Sensitivity modelling with objective damage assessment of unreinforced masonry façades undergoing different subsidence settlement patterns. Eng. Struct. **286**, 116113 (2023). https://doi.org/10.1016/j.engstruct.2023.116113
44. Rotunno, T., Fagone, M., Ranocchiai, G., Grande, E.: Micro-mechanical FE modelling and constitutive parameters calibration of masonry panels strengthened with CFRP sheets. Compos. Struct. **285**, 115248 (2022). https://doi.org/10.1016/j.compstruct.2022.115248
45. Shadlou, M., Ahmadi, E., Kashani, M.M.: Micromechanical modelling of mortar joints and brick-mortar interfaces in masonry Structures: a review of recent developments. Structures **23**, 831–844 (2020)
46. Shin, H.V., Porst, C.F., Vouga, E., Ochsendorf, J., Durand, F.: Reconciling elastic and equilibrium methods for static analysis. ACM Trans. Graph. (TOG) **35**(2), 1–16 (2016). https://doi.org/10.1145/2835173
47. Xia, Q., Sun, Y., Wu, J., Li, J., Li, Y., Shen, C.: Investigation of compression constitutive relationship of ancient brick masonry. Constr. Build. Mater. **317**, 126093 (2022). https://doi.org/10.1016/j.conbuildmat.2021.126093